Advanced Interferometry Techniques for Burning Plasmas

D.L. Brower, W.X. Ding

Department of Physics
University of California at Los Angeles
Los Angeles, California 90095-1547 USA

V.V. Mirnov

Department of Physics
University of Wisconsin-Madison
Madison, Wisconsin 53706 USA

M.A. Van Zeeland, T.N. Carlstrom

General Atomics
San Diego, California 92121-1122 USA

Abstract. For future burning plasma experiments, all diagnostics must be re-evaluated in terms of their measurement capabilities and robustness to the new environment. This is certainly true for interferometry measurements where conventional approaches may not be ideal and interpretation may require modification due to high plasma temperatures. Optimizing these systems to provide maximum information will be crucial to understanding burning plasma dynamics. This paper will explore a variety of phase measurement techniques for the main body and divertor regions that can be utilized on burning plasma experiments like ITER and beyond.

Keywords: interferometry, polarimetry, Faraday rotation, diagnostics
PACS: 52.55.Fa, 52.70.Gw, 52.70.Nc

INTRODUCTION

For future burning plasma experiments, all diagnostic systems need to be re-evaluated in terms of their measurement capabilities and robustness to the new environment. This is particularly true for interferometry measurements where conventional approaches may not be ideal and interpretation may require modification. On ITER, it is presently planned to have three interferometer systems playing multiple measurement roles. First, a tangential interferometer-polarimeter is required primarily to measure the line-integrated electron density for fueling control through realtime density feedback. Second, a poloidally-viewing interferometry-polarimetry system is desired to determine the internal magnetic filed structure and current density for evaluation of plasma safety factor profile, q, and its temporal evolution. Both of the above mentioned systems also provide internal density and magnetic constraints for

equilibrium reconstruction. Third, a divertor interferometer is planned to measure the electron density distribution along each divertor leg and to monitor the strike point. Each of these systems will need high time response in order to track fast dynamic events associated with ELMs, pellets, and disruptions. In addition, at least for the core plasma systems, it is hoped that these instruments can also measure fluctuations associated with magnetohydrodynamic (MHD) instabilities like tearing modes (or NTMs), Alfvenic modes, and even broadband turbulence. Optimizing each of these systems to provide maximum information will be crucial to understanding burning plasma dynamics. This is particularly critical in view that many standard diagnostic techniques presently employed in high-performance plasmas may no longer be feasible in the burning plasma environment.

A burning plasma represents an unknown and certainly difficult environment in which diagnostic systems need to reliably operate. The environment is extremely harsh as high energy neutrons and high levels of radiation impact various diagnostic components. Erosion of and deposition on optical components, plasma dust accumulation, and radiation-induced EMFs are a few of the issues that must be addressed. In addition, technology issues are critical. For example, realtime feedback alignment of optical systems is required for the up to 1000 sec discharge pulse lengths in ITER where thermal expansion can be of order several centimeters. Diagnostic integration into the overall machine design and port structure also represent serious issues that must be dealt with. Finally, temperatures in burning plasmas will be in the range 10-25 keV where measurements have not previously been made and assumptions regarding the plasma dielectric response (e.g., cold plasma approximations) may no longer be valid. This will affect interpretation of experimental results and the ability of instruments to meet the specified measurement requirements.

The scope of this work does not allow us to address all of these issues. Herein, we will focus the discussion on a variety of phase measurement techniques for the main body and divertor regions that can be utilized on burning plasma experiments like ITER and beyond. These techniques will go beyond those typically considered for interferometry diagnostics. In addition, the consequences of finite electron temperature on the plasma dielectric response will be considered by evaluating the contributions of both dispersive and relativistic effects. Finally, we will address expansion of the diagnostic capabilities to measure new equilibrium and fluctuating quantities, including fluctuations and the fluctuation-induced fluxes.

INTERFEROMETRY TECHNIQUES

In this section we will briefly examine various interferometry techniques and their applicability to burning plasma experiments like ITER. In the context of this paper, a broad definition of interferometry is utilized whereby we refer to any phase measurement as an interferometry technique. This class of measurement then includes conventional interferometry (and variations like dispersion and differential interferometers), Faraday rotation, Cotton-Mouton effect, and Fizeau interferometry.

Conventional Interferometry

In the conventional interferometer setup (see Fig. 1), one uses probe (Laser1) and local oscillator (LO) beams (Laser 3) that mix in both the signal and reference detectors. Since the linearly-polarized laser beams are at difference frequency $\Delta\omega = \omega_1 - \omega_3$ (where $\omega >> \omega_{pe}$ and ω_{ce}), the output of each detector is a sinusoid waveform at $\Delta\omega/2\pi \sim 1$ MHz. By measuring the phase difference between the waveforms from the two mixers, one can determine the plasma induced phase shift due to the fact that the beam path for the signal mixer traverses the plasma. The resulting phase measurement ϕ can then be related to the plasma density according to the relation $\phi(rad) = 2.8 \times 10^{-15} \lambda \int n_e dL$, where λ is the laser wavelength, n_e the electron density and dL the path length through the plasma (mks units). In the above relation, it is assumed that (1) magnetic field can be ignored, (2) the plasma is stationary, (3) and temperature effects are unimportant.[1]
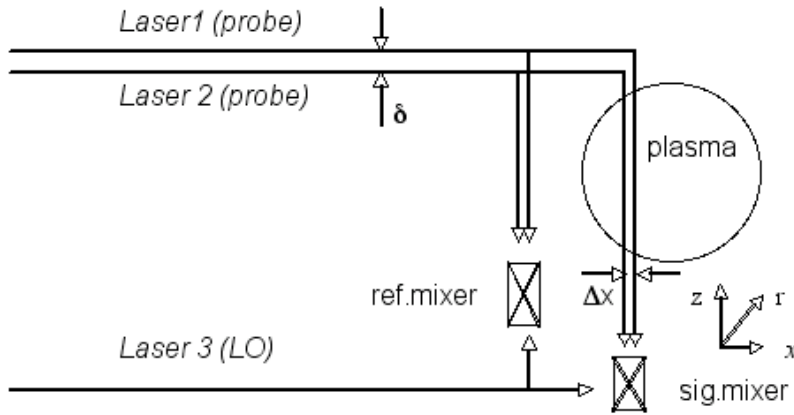

FIGURE 1. Experimental layout for various interferometer systems.

However, if path length changes (such as those due to thermal expansion or vibrations) do occur, an extra phase term that goes as $\Delta L/\lambda$ must be included. If this term is large, additional information is required to resolve the plasma density. This can by accomplished by adding an additional probe beam (Laser2 in Fig. 1) with spatial offset δ=0. If one now rewrites the measured phase for each probe beam, we end up with a system of 2 equations and 2 unknowns,

$$\phi_{\lambda_1} = c_I \lambda_1 \int n_e dL + \frac{2\pi\Delta L}{\lambda_1} \quad and \quad \phi_{\lambda_2} = c_I \lambda_2 \int n_e dL + \frac{2\pi\Delta L}{\lambda_2},$$

and can solve for the line-averaged plasma density.[2] This approach is commonly referred to as 2-color interferometry. The two laser wavelengths are typically chosen to be far apart (one more sensitive to plasma and the other to path length) as this optimizes the density resolution which can be written as

94

$$\delta n_e L = \frac{\delta \phi}{r_e(\lambda_1 - \lambda_2)},$$

where r_e is the classical electron radius, $\delta\phi$ is the diagnostic phase resolution and δn_e is the resulting density resolution. This approach is commonly used on high performance tokamak devices. A drawback of this approach is that often both plasma and the path length change terms are much greater than a fringe ($>>2\pi$ phase change) making the system vulnerable to fringe skip errors and hence potentially unreliable for realtime density feedback control of burning plasmas. Various post-signal processing approaches[3] can be employed to minimize this error but it is still desirable to develop a more robust technique.

Dispersion Interferometer: One way the phase ambiguity associated with fringe counting errors can be remedied is by employing the dispersion interferometer technique.[4] This approach is a variation of the 2-color interferometer approach where Laser1 (Fig. 1) passes through a frequency doubler and converts part (depending on efficiency) of ω_1 into $2\omega_1(=\omega_2)$. These two beams are collinear (δ=0) and both traverse the plasma. After leaving the plasma, there is a second frequency doubler which again converts part of the remaining ω_1 into $2\omega_1(=\omega_2)$. The frequency doubler also doubles the phase making the phase difference between the 2 probing beams equivalent to $\Delta\phi = 2\phi_{\omega_1} - \phi_{2\omega_1} = \frac{3\lambda}{2}c_I\int n_e dL$. When phase is doubled, the path length change term is identical for each frequency and cancels out before the phase measurement leaving only the plasma term. This technique was successfully tested on the TEXTOR tokamak providing a line-integrated resolution of $\delta n_e dL \approx 2 \times 10^{17}\ m^{-2}$.[5] Since the path length change term is often the source of fringe counting errors, being many hundreds of fringes, this approach significantly improves system reliability. The plasma-induced phase change can still be $>>1$ fringe and a source of fringe counting error. However, in the ITER divertor, for most plasma scenarios envisioned the plasma-induced phase is <1 fringe (for 10.6 μm interferometer) making the dispersion interferometer immune to fringe counting errors even if the signal is temporarily lost.[6]

Differential Interferometer: Another approach to removing fringe counting errors is the differential interferometer.[7] From conventional interferometry, the density profile is found by performing a standard Abel inversion using

$$n_e(r) = -\frac{1}{\pi r_e \lambda}\int_r^a \frac{\partial\phi(x)}{\partial x}\frac{dx}{\sqrt{x^2 - r^2}},$$

where x is the impact parameter (cylindrical geometry). From this relation it is clear that the first spatial derivative of the phase, $\partial\phi/\partial x$, is required to obtain $n_e(r)$. Conventional interferometers measure $\phi(x)$ for multiple discrete chords, make a numerical fit to the available points, take the spatial derivative to infer $\partial\phi/\partial x$, and then perform an inversion. A difficulty in directly measuring $\partial\phi/\partial x$ is that the phase difference becomes smaller as two adjacent chords are brought closer together. However, phase noise due to vibrations and other effects can be minimized if both probe beams use the same optics. By taking advantage of the reduced phase noise,

measurement of small phase difference becomes feasible. This approach was used to to directly measure $\partial\phi/\partial x$ at multiple spatial points and then invert to obtain the local density profile. Two separate laser beams (Laser1 and Laser2 in Fig. 1) with slight spatial offset δ and frequency difference Δω are coupled into a single mixer making a heterodyne measurement of the phase difference which is <1% of the total phase change experienced by each beam separately. This measure of the differential phase is made at multiple spatial points and can be inverted directly to provide the local density distribution.
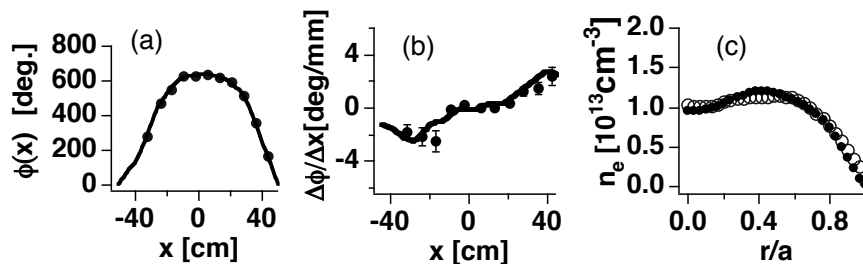

FIGURE 2. (a) Measured phase profile φ(x) for conventional interferometer (solid circles); Solid line is spline fit to measured points; (b) First derivative of phase, dφ/dx, is calculated and shown as solid line. Direct measurements by differential interferometry at the same chord locations as (a) are shown by solid circles for δ=1.2 mm; (c) Inverted density profile comparison using the conventional (open symbols) and differential (solid symbols) interferometer techniques.

The phase gradient $\Delta\phi/\Delta x$ from a differential interferometer measurement is shown in Fig. 2(b). The width of each Gaussian laser beam is ~10 mm and the spatial offset $\Delta x(=\delta)$~1.2 mm. This parameter can also be obtained numerically by fitting φ(x) (in Fig. 2(a)) and taking the derivative as plotted in Fig. 2(b). Both give consistent results within experimental errors. For purposes of comparison, the density profiles obtained using the conventional interferometer and differential interferometer measurements are shown in Fig. 2(c). The agreement is not surprising since the two interferometric techniques produced the same $\Delta\phi/\Delta x$ profile. The advantage of the differential technique is that while the phase φ>1000°, the differential phase <4° for all chords (even the steep gradient regions). Consequently, while the conventional interferometer is subject to fringe skips, the differential is not.

Faraday Rotation

Faraday rotation results from birefringence along the field in a magnetized plasma and can be expressed as the phase difference between R- (right hand circularly polarized) and L-wave (left hand circularly polarized) refractive indices according to

$$\psi_{Faraday} = \frac{1}{2}\int (k_L - k_R)dL = \int \frac{\omega}{2c}(N_L - N_R)dL \approx \int \frac{\omega_{pe}^2 \omega_{ce}\cos\theta}{2c\omega^2}dL \sim 2.62\times10^{-13}\lambda^2 \int n_e B_{//}dL,$$

where $B_{//}=B\cos\theta$ is the component of the magnetic field along the laser beam. (Referred to as Faraday rotation since an initially linear wave would have its polarization axis rotated according to the above relation.) Measurements can be

96

realized schematically as shown in Fig. 1, where Laser1 and Laser2 have offset δ=0 with R- and L- wave polarizations, respectively. Since the two beams are collinear, path length changes and vibration effects automatically cancel since the two beams have wavelength difference $\Delta\lambda/\lambda \approx 10^{-6}$ (i.e., frequency offset only for heterodyne detection). Plasma phase shifts for wavelengths of interest are $\ll 2\pi$, thereby making such measurements immune to fringe counting errors. For a poloidally-viewing system, Faraday rotation measurements provide information on the poloidal magnetic field and toroidal current density which is critical to evaluating the q profile in burning plasmas.[8] Simultaneous measurement of electron density can be made along the same chords.[9]
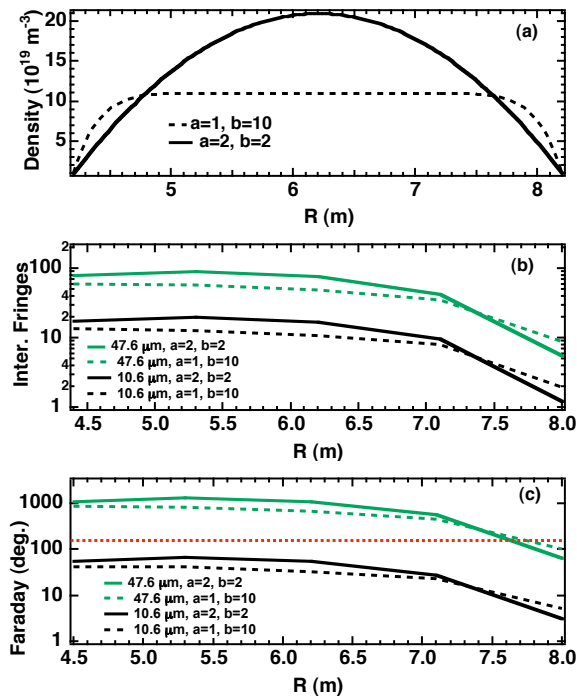

FIGURE 3. (a) Density profiles as a function of major radius for peaked profile (solid line) at $\sim 2\text{xn}_{GW}$ (*a=2,b=2*) and flat profile (dashed line) at $\sim n_{GW}$ (*a=1, b=10*). Double-pass tangential (b) interferometer and (c) Faraday rotation phase [x2] as a function of tangency radius for 47.6 (green) and 10.6 μm (black) laser radiation. Horizontal red dashed line corresponds to a single fringe in (c).

For a tangentially-viewing system, Faraday rotation can be used to determine the electron density as the toroidal magnetic field is largely known for the tokamak configuration.[10] This approach has been selected for ITER in combination with a 2-color interferometer. To provide an estimate of the anticipated phase shifts, we take a density profile described by $n_e = a \times 10^{20}[1-(r/a_o)^b]$ m^{-3}, where for simplicity we employ a circular plasma cross section with minor radius $a_o = 2$ m and major radius $R_o = 6.2$ m. The resulting density for cases of high-density peaked [a=2,b=2] and low-

97

density flat [a=1,b=10] profiles are shown in Fig. 3(a). For ITER, the Greenwald density limit is n_{GW}~1.2 x 10^{20} m^{-3}, making steady-state operation at densities above 2-3xn_{GW} unlikely. However, during disruption mitigation phases of operation the density may reach as high as 10^{22} m^{-3}. The calculated interferometer and Faraday rotation phase shifts for laser radiation at 10.6 and 47.6 μm are shown in Fig. 3(b) and (c). Here we immediately see that the plasma-induced interferometer phase shifts (not including path length changes) are many fringes at each wavelength. For Faraday rotation, only the 10.6 μm choice gives phase change <2π for both density scenarios. This makes a 10.6 μm laser source the likely choice for ITER as it will be better suited to providing error-free operation.

Cotton-Mouton Effect

The Cotton-Mouton effect results from birefringence perpendicular to the field in a magnetized plasma and can be expressed as the phase difference in the O- (ordinary) and X-wave (extraordinary) refractive indices according to the relation

$$\psi_{CM} = \int (k_O - k_X)dL = \int \frac{\omega}{c}(N_O - N_X)dL \approx \int \frac{\omega_{pe}^2 \omega_{ce}^2}{2c\omega^3} dL \sim 2.45 \times 10^{-11} \lambda^3 \int n_e B_\perp^2 dL \quad ,$$

where $B_\perp$ is the component of the magnetic field perpendicular to the laser beam propagation direction. (The Cotton-Mouton effect changes an initially linear wave to elliptical polarization.) Measurements can be realized according to Fig. 1 where Laser1 and Laser2 have offset δ=0 with linear but perpendicular wave polarizations. Since the two beams are collinear, path length changes and vibration effects automatically cancel the same as for Faraday rotation. Typically plasma phase shifts, for wavelengths of interest, are <<2π, thereby making such measurements immune to fringe counting errors. For ITER, a Cotton-Mouton effect polarimeter is under consideration for the divertor legs as $B_\perp$ is the known toroidal field.[6] Estimates of anticipated phase shifts are shown in Fig. 4. Longer wavelength is necessary to obtain a sufficiently large phase shift. This measurement has been successfully demonstrated on the WVII-AS stellarator.[11]
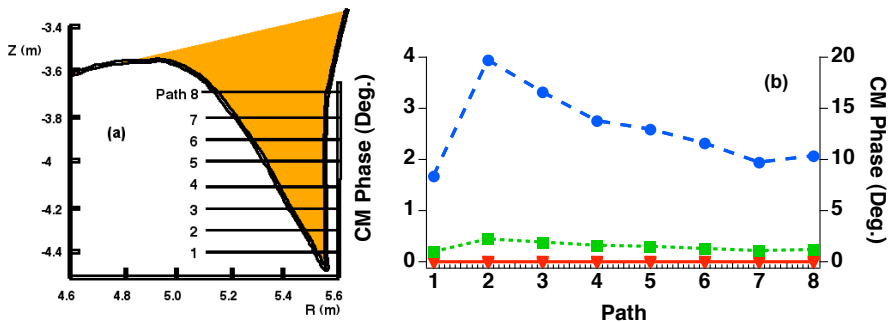

FIGURE 4. (a) Lines-of-sight for ITER outer divertor leg, (b) Estimate of Cotton-Mouton phase for λ= 118 (circles), 57 (squares) and 10.6 (triangles) μm radiation for baseline case -1.8 x 10^{21} m^{-3} (left vertical axis) and high density case - 1 x 10^{22} m^{-3} (right vertical axis).

Fizeau Interferometer

The Fizeau effect is the relativistic phase shift of an electromagnetic wave associated with movement of a dielectric medium. In a moving electron fluid, the phase shift experienced by an electromagnetic wave including Fizeau effect is

$$\phi^{'} = \phi + \alpha = \phi + \frac{1}{\omega c^2} \int v_e \omega_{pe}^2 dL = \phi + 1.875 \times 10^{-23} \lambda \int n_e v_e dL \ ,$$

where v_e is the electron velocity along the laser beam and $\phi(rad) = 2.8 \times 10^{-15} \lambda \int n_e dL$, the conventional interferometer phase shift. The additional term α is the Fizeau phase shift and is dependent of the direction and magnitude of electron velocity. By devising a counter-propagating interferometer,[12] the Fizeau effect phase can be isolated. In such a configuration, Laser1 and Laser2 in Fig. 5 would be linearly-polarized, counter-propagating, colinear ($\delta=0$) beams with phase difference proportional to 2α. A single-pass tangential Fizeau interferometer phase shift for ITER parameters using a 10.6 μm laser is ~0.5-2°, depending on plasma conditions. Multiplying the Fizeau phase shift by the electron charge provides a line-integrated measure of the toroidal electron current density. The Fizeau measurement is insensitive to path length changes.
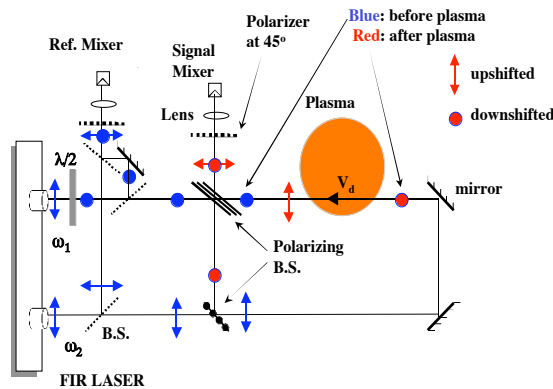

FIGURE 5. Experimental arrangement for measuring the Fizeau effect.

Finite Temperature Effects

All interferometer and polarimeter phase shifts discussed to this point are based on the cold plasma dispersion relation (i.e., $T_e=0$). ITER will operate at electron temperatures in the range T_e~10-25 keV motivating us to reexamine the cold plasma assumption. Finite thermal (or nonrelativistic dispersive) effects essentially increase the electron plasma frequency and, therefore, the measured phase is larger than for a cold plasma. However, relativistic effects dilate the electron mass which decreases the plasma frequency and reduces the measured phase. The combined effect has recently been approximated analytically by Mirnov[13] for temperatures and frequencies appropriate

99

for ITER, where the phase correction factors become approximately $(1 - \frac{3}{2}\frac{T_e}{m_e c^2})$ for interferometry and $(1 - 2\frac{T_e}{m_e c^2})$ for Faraday rotation. Measured phase shifts for interferometry and polarimetry including temperature effects can be written as

$$\phi = c_I \int n_e (1 - \frac{3}{2}\frac{T_e}{m_e c^2}) dl = c_I \int n_e dl - \frac{3}{2}\frac{c_I}{m_e c^2} \int n_e T_e dl \qquad (1)$$

$$\psi_{Faraday} = c_F \int n_e B_{//} (1 - 2\frac{T_e}{m_e c^2}) dl = c_F \int n_e B_{//} dl - \frac{2c_F}{m_e c^2} \int n_e T_e B_{//} dl \qquad (2)$$

where c_I and c_F are constants. For T_e=15 keV, the correction is 4.4% for interferometery and 6% for polarimetry, respectively. This means that an interferometer interpreted using the cold plasma dispersion relation would underestimate the central density by 4.4%.
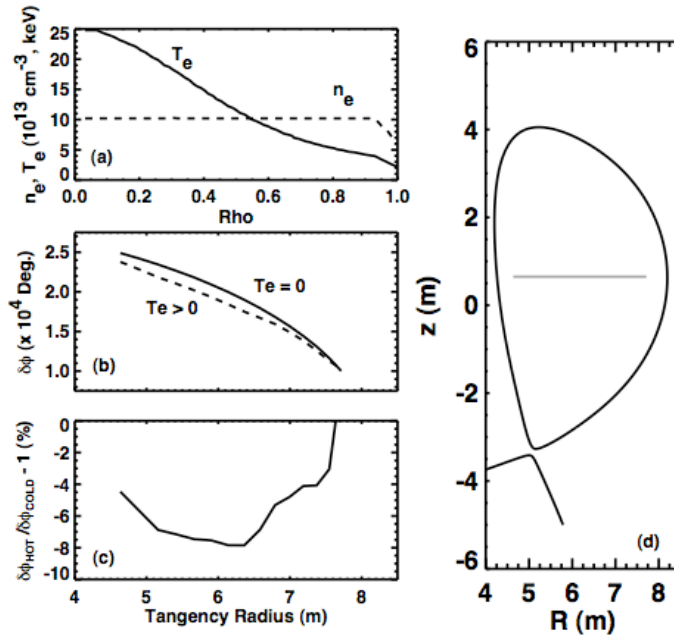

FIGURE 6. GENRAY calculations for the ITER. (a) Input electron temperature and density profiles. (b) Interferometric phase shift for cold plasma (solid) and fully relativistic dispersion relation (dashed). (c) Relative difference between finite temperature and cold plasma interferometric phase shift shown in (b). (d) Equilibrium shape of ITER scenario 2 plasma.

Equation (1) above has been verified numerically using the GENRAY code and the full hot plasma relativistic dispersion relation[14] for a variety of plasma conditions and

wavelengths. An example GENRAY calculation of the interferometer phase shift for a 25 keV ITER plasma and a 57 micron probing beam is shown in Figure 6(b). For reference, the electron density and temperature profiles, as well as the equilibrium profile used are shown in Figs. 6(a) and (d), respectively. Both the finite temperature (dashed) and cold plasma (solid) results are given in Fig. 6(b), while the relative difference is shown in Fig. 6(c). The interferometry phase error varies from 0 to 8% across the profile. The net effect of the finite temperature effect is a decrease in the interferometric phase shift – as expected from Eq.(1).

Since temperature is known from Thomson scattering, finite T_e effects can be corrected. Alternatively, for a tangential Faraday system where B_ϕ is largely known, the above two equations have only two unknowns and hence provide information on both the plasma electron density and temperature. One can then directly determine the plasma electron pressure profile. Finite temperature effects must be considered for all interferometry techniques used in the high-temperature burning plasma environment.

Fluctuation Measurements

For all the interferometry techniques discussed, it is possible to make measurements with both high phase resolution and high time response. This combination permits measurement of both fast changes to the equilibrium profiles as well as fluctuations. As an example, a fast, laser-based Faraday rotation diagnostic has been employed to measure both the line-integrated wavenumber and frequency spectrum of radial magnetic field fluctuations in the high-temperature plasma core, as shown in Fig. 7. Such measurements can be used on ITER or future burning plasmas to monitor core MHD fluctuations associated tearing modes, fast particle driven Alfvenic modes and even broadband turbulence. Combined Faraday rotation and interferometry measurements can be used to get local information on δn, $\delta b_{r,\theta,\phi}$, $\delta j(\omega,k)$, their coherence, phase relation and even the fluctuation-induced flux.[15,16,17]
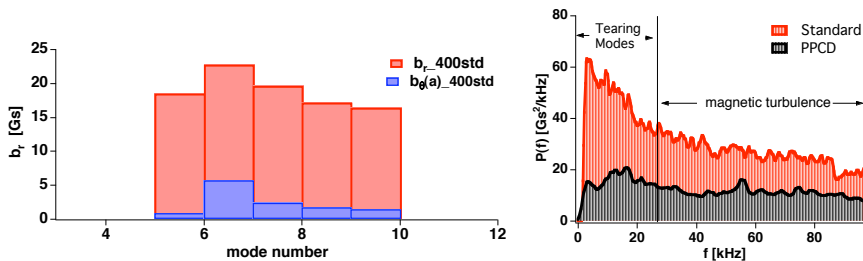

FIGURE 7. Radial magnetic field fluctuation line-integrated wavenumber and frequency spectra for standard (std) and high confinement (PPCD) plasmas.

101

REFERENCES

[1] I.H. Hutchinson, Principles of Plasma Diagnostics, Cambridge University Press (Cambridge, UK) 2002.

[2] Yasunori Kawano, et al., Rev. Sci. Instrum. **63**, 4971(1992).

[3] A. Murari et al., Rev. Sci. Instrum. **77** 073505 (2006).

[4] V.P. Drachev, et al., Rev. Sci. Instrum. **64**,1010(1993).

[5] P.A. Bagryansky, et al., Rev. Sci. Instrum. **77**,053501(2006).

[6] D.L. Brower, W.X. Ding, B.H. Deng, Rev. Sci. Instrum. **77**,10E911(2006).

[7] W.X. Ding, D.L. Brower, B.H. Deng, T. Yates, Rev. Sci. Instrum. **77**, 10F105(2006).

[8] A.J.H. Donne, et al., Rev. Sci. Instrum. **75**, 4694(2004).

[9] B.H. Deng, D.L. Brower, et al., Rev. Sci. Instrum. **77**,10F108(2006).

[10] R.T. Snider, et al., Rev. Sci. Instrum. **68**,728(1997).

[11] Ch. Fuchs and H.J. Hartfuss, Phys. Rev. Lett. **81**,1626(1998).

[12] D.L. Brower, et al., Rev. Sci. Instrum. **75**, 3399-3401(2004).

[13] V.V. Mirnov, W.X. Ding, D.L. Brower, M.A. Van Zeeland, T.N. Carlstrom, accepted for publication in Phys. of Plasmas (September, 2007).

[14] A.P. Smirnov, R.W. Harvey, Bull Amer. Phys. Soc. **39** 1626 (1994).

[15] N.E. Lanier, et al., Phys. Plasmas **8**,3402-3410(2001).

[16] W.X. Ding, D.L. Brower, et al., Phys. Rev. Lett. **99**,055004(2007).

[17] D.L. Brower, et al., Rev. Sci. Instrum. **74**, 1534-1540(2003).